Talanta 168 (2017) 82–90

Contents lists available at ScienceDirect

Talanta

journal homepage: www.elsevier.com/locate/talanta

Amplification of resonance Rayleigh scattering of gold nanoparticles by tweaking into nanowires: Bio-sensing of α-tocopherol by enhanced resonance Rayleigh scattering of curcumin capped gold nanowires through non-covalent interaction

Riham El Kurdi, Digambara Patra*

Department of Chemistry, American University of Beirut, Beirut, Lebanon

ARTICLE INFO

Keywords:
Biosensors
Resonance Rayleigh Scattering
α-Tocopherol
Au NWs

ABSTRACT

Tuning optical properties by controlling size and shape of the metallic nanoparticles has been of great interest to design novel bio-sensing techniques. Here, as a first example we illustrate that resonance Rayleigh scattering (RRS) signal of Au nanoparticles (NPs) can be amplified > 10-fold by growing into Au nanowires (NWs). These thin and long NWs of ~20–25 nm diameter and > 1 μm length can be achieved by suitably manipulating the temperature during green synthesis using curcumin. Interestingly, mixture of Au NWs and NPs or shorter NWs gives a moderate increase in RRS signal suggesting formation of longer NWs is crucial for optimal enhancement of RRS signal. Curcumin along with CTAB act as capping and stabilizing agent for Au NWs/NPs in different temperatures, which is confirmed by XRD, TGA, DSC, EDX and FT-IR data. This amplified RRS signal of Au NWs has been employed to design a new optical biosensor for α-tocopherol (α-TOH), which is among the most biologically active form of vitamin E. Association of α-TOH with Au NWs further enhances the RRS signal of Au NWs, ~10 fold through non-covalent interaction. No interference from other antioxidant substances like ascorbic acid and 6-O-Palmitoyl-L-ascorbic acid is observed. The sensing method is simple, fast and offers remarkable linear dynamic ranges, 12.8–1004 μmol L^{-1}, which is larger than reported values. The detection limit for α-TOH estimation has been found to be 50 nmol L^{-1}. The biosensor is found to be stable both in the absence and presence of α-TOH and provides an excellent recovery for synthetic samples.

1. Introduction

Nanoparticles have proven to be the most flexible structures owing to the synthetic control of their size, shape, composition, structure, assembly and encapsulation, which result in tuning their optical properties [1–7]. Optical properties can be tuned by controlling size and shape of metallic nanoparticles (NPs). Different shapes can be achieved by using several synthetic methods and by varying multiple parameters, such as, concentration of the reactants, reaction conditions, temperature and the nature of solvent [8–11]. Au NPs have shown promises in biomedicine domain, biological imaging, genomics, clinical chemistry, and diagnostic tests [5,12–15]. Due to their unique optical properties, colloidal Au NPs present a significant role in biomedical applications, remarkably in the area of cancer photo-diagnostics and phototherapy [16]. Recent advances in molecular specific cancer detection and therapy using Au NPs have led to the development of new techniques including light scattering imaging [17–19], 2-photon luminescence imaging [20–22], surface enhanced Raman scattering [23–25] and plasmonic photo-thermal therapy [26–28].

At the same time, new green chemistry strategies to generate Au NPs without using toxic chemicals are being actively considered for their biomedical applications [29–38]. Curcumin, a major component of turmeric, is not toxic and safe. It has shown effective therapeutic properties as an anti-inflammatory drug [39], chemo-preventive [40], antioxidant [41], etc. The last two decades have generated much enthusiasm among researchers to explore application of curcumin for its beneficial biological and pharmacological activities [42–44]. A number of reports have shown the ability of curcumin to inhibit free radical species generation, which is attributed to the abstraction of H atom from C_{12} methylene group or from phenolic groups [45,46]. Therefore, in our earlier work we have applied curcumin to prepare Au NPs or nanorods through a green approach towards biomedical applications [47–50].

* Corresponding author.
E-mail address: dp03@aub.edu.lb (D. Patra).

http://dx.doi.org/10.1016/j.talanta.2017.03.021
Received 11 January 2017; Received in revised form 6 March 2017; Accepted 7 March 2017
Available online 09 March 2017

Tocopherols are the major components of vitamin E [51]. α-Tocopherol (α-TOH) is the most common group of tocopherols and is known as vitamin E. α-TOH has been associated with sterility and reproduction. Recently there has been increased interest in the use of α-TOH isolated from wheat germ oil as an antioxidant in food processing. It has been established that α-TOH is essential for the integrity and optimal function of all mammalian cells [52–54]. α-TOH has also many important functions and natural phenolic anti-oxidant properties. It is responsible for many of the healthful properties in foods, which include vegetable oils, milk, fruits etc. α-TOH has high nutritional properties and it helps to prevent oxidation of lipids that would ensure the establishment of undesirable compounds producing oil deterioration [55]. As a fat-soluble antioxidant, it interrupts the propagation of reactive oxygen species that spread through biological membranes or through a fat when its lipid content undergoes oxidation by reacting with more-reactive lipid radicals to form more stable products. For this reason, the development of simple and sensitive methods for the detection of α-TOH has attracted considerable interest.

There is a growing interest to develop bio-sensing scheme for α-TOH. Various methods have been reported for the determination of α-TOH. These techniques include gas chromatography, HPLC, capillary electrophoresis, and electrochemical methods [55–58]. Most of these methods have major limitations as they need excessive sample pretreatment and separation procedures. Some of them like GC and HPLC are time consuming and need solvent extraction, solid-phase extraction or saponification. Few of them need extraction steps prior to the analysis. HPLC is also an expensive equipment and considerable skill is required to operate the technique successfully. In addition, liquid chromatographic methods necessitate high strength ionic buffered mobile phase that are hazardous for column efficiency and require prolonged time for column saturation and washing. Other possible bio-sensing techniques like electrochemical methods suffer due to poor sensitivity and complex chemical manipulations. Direct Resonance Rayleigh Scattering (RRS) method can be an alternative powerful tool to sense α-TOH quickly. But α-TOH scatter light poorly and it has no fluorescence properties. Therefore, there is little report on development of α-TOH using optical properties. Interestingly nanoparticles have unique chemical and physical properties, which are extremely suitable for designing new and improved sensing devices, especially optical sensors and biosensors. Gold nanoparticles have been found to be great sensors in biosensors and biomedicine applications. The bio-catalytic growth of gold nanoparticles has been employed in the design of new optical biosensors based on the enhanced RRS signals [59–61]. RRS signal from Au NPs has been successfully used for analytical method development [62].

In this work, we have prepared gold nanoparticles and nanowires through one pot green synthetic procedure using curcumin by manipulating temperature and shown that RRS signal of Au NPs can be further amplified by creating Au nanowires (NWs). In this case, temperature during synthesis of Au particles facilitates to control the size and shape of NWs. The curcumin capped Au NWs prepared at 45 °C are found to be thin and long [49], which offers enhanced RRS signal compared to spherical Au NPs prepared at 30 °C. The RRS signal of curcumin capped Au NWs has been exploited to develop an easy and fast sensing scheme for the estimation of α-TOH, where association of α-TOH with Au NWs further boost RRS signal. To our knowledge, the proposed bio-sensing method is the first of its kind where RRS technique as well as Au NWs have been successfully used for the determination of α-TOH. The method gives remarkable linear dynamic ranges, which is larger than reported values. The biosensor is found to be stable both in the absence and presence of α-TOH and offers excellent recovery for synthetic samples.

2. Materials and methods

2.1. Materials

Gold (III) chloride hydrate (99.999% trace metal basis), curcumin and silver nitrate were obtained from Sigma Aldrich. Cetyltrimethylammonium bromide (CTAB) was received from Acros Organics. Similarly, α-tocopherol was purchased from Sigma Aldrich, ascorbic acid and 6-O-Palmitoyl-L-ascorbic acid were from Fluka. All the chemicals were used directly without further purification and were dissolved in double distilled water except for curcumin, α-tocopherol and 6-O-palmitoyl-L-ascorbic acid, which were initially dissolved in methanol to prepare stock solutions.

2.2. Synthesis of Au NPs/NWs

The preparation of gold nanoparticles/nanowires was made by dissolving 0.27g of CTAB in 15 mL of double distilled water heated at 60 °C and the solution was kept for 2 min in water at 30 °C. Subsequently, the solution was kept for 15 min at 30 °C after adding 1 mL of 4 mmol L^{-1} $AgNO_3$, which was followed by the incorporation of the 1 mmol L^{-1} gold solution dissolved in 15 mL DDW. The synthesis was done in basic media for that reason 1 mL of NaOH at pH=13 was added and stirred for 2 min at 400 rpm as shown in Scheme 1A. The final solution was kept for 24 h in four different temperatures, 30, 45, 60 and 75 °C for the preparation of different size and shape nanoparticles/nanowires, thus, the incubation temperatures were 30, 45, 60 and 75 °C, respectively. To end up the reaction procedure, the solution was centrifuged at 1000 rpm for 5 min and 15,000 rpm for 25 min to precipitate the gold particles (see Scheme 1B). For production of nanowires and sensing measurement, incubation temperature was 45 °C.

2.3. Characterization and spectroscopic analysis

The absorption spectra were recorded at room temperature using a JASCO V-570 UV–VIS–NIR spectrophotometer. The X-Ray diffraction (XRD) data were collected using a Bruker d8 discover X-Ray diffractometer equipped with Cu-Kα radiation (λ=1.5405 Å). The monochromator used was Johansson Type. Scanning electron microscopy (SEM) analysis was done using Tescan, Vega 3 LMU with Oxford EDX detector (Inca XmaW20). In short, few drops of gold solution were deposited on an aluminum stub and coated with carbon conductive adhesive tape. FT-IR spectra were recorded on a FT-IR-Raman spectrometer. A Thermo Nicolet 4700 Fourier Transform Infrared Spectrometer equipped with a Class 1 laser was used for this purpose. The KBr pellet technique was applied to perform the transmission experiments in the range between 3200 and 500 cm^{-1}. The Thermogravimetric Analysis (TGA) and Differential Scanning Calorimetry (DSC) measurements were done using a Netzsch TGA 209 in the temperature range 30–800 °C with an increment of 10 °C min^{-1} in a N_2 atmosphere. Synchronous fluorescence scan was measured using Jobin-Yvon-Horiba Fluorolog III fluorometer and the FluorEssence program. The excitation source was a 100 W Xenon lamp, and the detector used was R-928 operating at a voltage of 950 V instrument by keeping the excitation and emission wavelength interval ($\Delta\lambda$) at 0 nm.

2.4. Sample for bio-sensing

Stock solution of 10 mmol L^{-1} of α-TOH was prepared. For stock solution, ascorbic acid was dissolved in double distilled water whereas α-TOH and palmitoyl ascorbic acid were dissolved in methanol. Several solutions were prepared with known concentration in the range 0–1 mmol L^{-1} by keeping the concentration of Au NWs constant in a total volume of 3 mL.

3. Results and discussion

For the preparation of Au NWs/NPs, green synthesis was performed in double distilled water at pH=13 and at an adequate temperature as shown in Scheme 1. The use of CTAB in green synthesis had a primary role in the gold reduction from Au^{3+} to Au NPs by

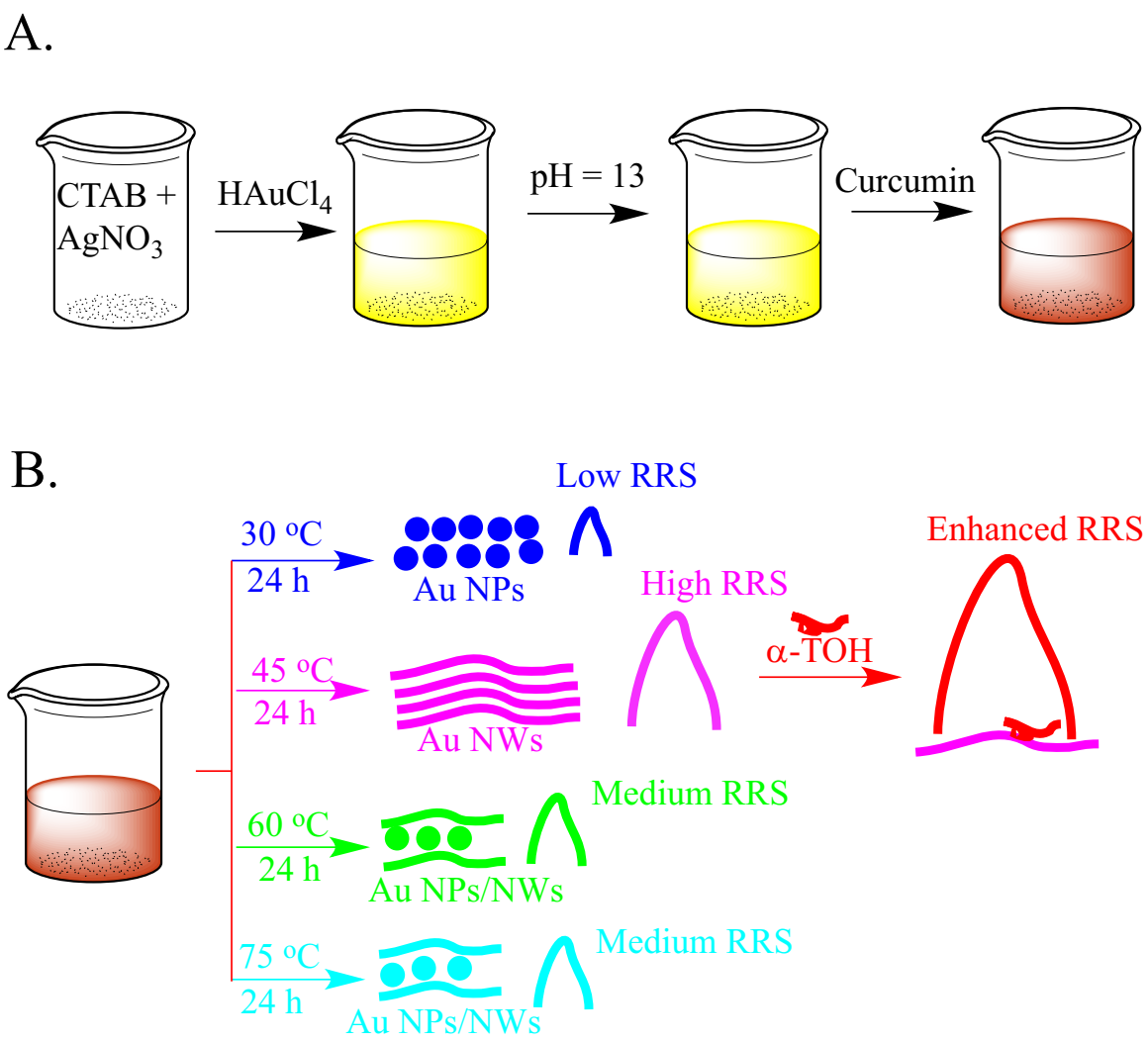

Scheme 1. (A) Scheme for general green synthetic procedure during preparation of gold particles by reducing Au^{3+} using curcumin in CTAB media; (B) Illustration of formation of gold nanowires (Au NWs) and gold nanoparticles (Au NPs) at different temperatures showing low, medium and high Resonance Rayleigh Scattering (RRS) signal. Right hand side in the scheme shows enhancement of high RRS signal of Au NWs in the presence of α-tocopherol (α-TOH).

curcumin. In addition, CTAB was useful in solubilizing hydrophobic curcumin. During synthesis, four different temperatures were tested, such as, 30, 45, 60 and 75 °C. The temperature had a significant influence on the SPR bands of formed Au particles, where a blue shift was noticed while going from 30, 60 and 75 °C to 45 °C. Although the absorption spectrum of curcumin has two strong absorption bands, one in the visible region with maximum ranging from 410 to 430 nm ($S_0 \rightarrow S_1$ transition) and another band in the UV region with maximum at 265 nm($S_0 \rightarrow S_2$) region, the absorption maximum of fully deprotonated (red in color) curcumin in alkaline pH (> pH 10) is at 467 nm [63]. Gold nanoparticles provide strong SPR bands in the visible region, for example, Au NPs show the SPR band ~520 nm, which is affected by the particle size due to the fact that at the LSPR wavelength gold nanoparticles exhibit an enormous electric field enhancement extended from their surface [64,65]. Therefore, UV–visible spectral measurement was initially applied to confirm synthesis of Au NPs/NWs. When synthesis was carried out at 45 °C a clear peak was obtained at 546 nm as shown in Fig. 1A. This peak shifted to 510, 508 and 482 nm at 30, 60 and 75 °C respectively. In fact, increasing particle size blue shifted the SPR wavelength and also increased the intensity.

Resonance Rayleigh Scattering (RRS) spectrum can be measured by applying synchronous fluorescence spectroscopy (SFS) by keeping the wavelength interval (Δλ) at 0 nm [66]. The RRS spectra of Au NPs obtained for the different temperatures are shown in Fig. 1B. The gold nanoparticles prepared in CTAB media at all the temperatures gave two major RRS peaks at ~377 nm and ~548 nm. However, for the particles prepared at 45 °C the intensity of the peak at 548 nm was enhanced, > 10 fold, compared to the particles prepared at 30 °C. The RRS signal for the particles prepared at 60 and 75 °C was intermediate. This change in RRS signal can be due to change in the size of the particles, which was later on confirmed from SEM images. The differences in the shape of the gold nanoparticles can be easily realized in the SEM images depicted in Fig. 2. In fact, at 45 °C, thin and long gold nanowires of 20–30 nm diameter and > 1 μm length were formed (Fig. 2B), similar to our earlier observation [49], whereas at 30 °C spherical Au NPs of 20–30 nm diameter were obtained (Fig. 2A). However, at 60 °C (Fig. 2C) and 75 °C (Fig. 2D) thin and short Au NWs of 20–30 nm diameter and 100–200 nm length along with spherical Au NPs of 20–30 nm diameter were obtained. The RRS signal of the prepared particles decreased in the following order: 45 °C > 60 °C > 75 °C > 30 °C, which suggests that smaller spherical Au NPs has low RRS signal, mixture of Au NWs and NPs or shorter NWs has moderate RRS signal and longer NWs has optimally enhanced RRS signal.

Formation of Au particles was established by EDX. EDX analysis illustrated the presence of Au peaks and carbon peak as expected due to capping of CTAB/curcumin and did not show any peak for Ag for all the

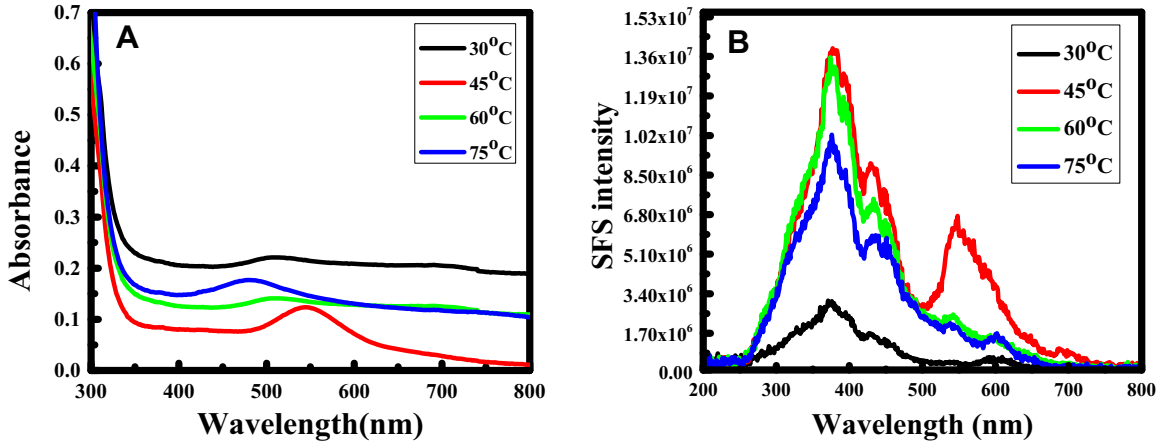

Fig. 1. (A) UV–Vis spectra of curcumin conjugated Au nanoparticles/nanowires prepared in four different temperatures. (B) Synchronous fluorescence spectra at Δλ=0 nm of curcumin conjugated Au nanoparticles/nanowires prepared in four different temperatures.

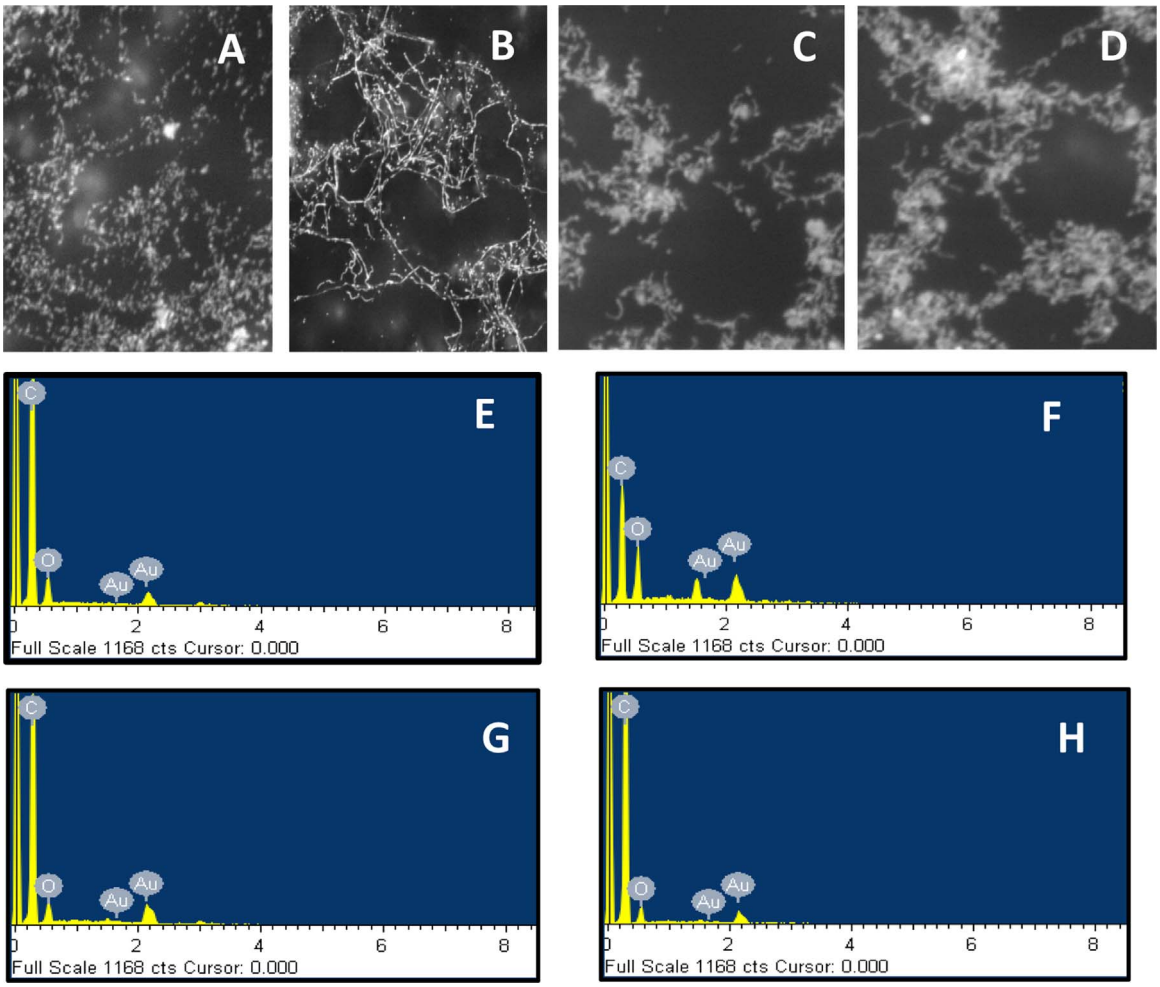

Fig. 2. SEM images of curcumin conjugated gold nanoparticles/nanowires prepared at 30 °C (A) with the relative EDX (E), 45 °C (B) with the relative EDX (F), 60 °C (C) with the relative EDX (G) and 75 °C (D) with the relative EDX (H).

fours samples prepared in different temperatures (see Fig. 2E–H). This concludes that silver nanoparticles were not formed during Au NPs/NWs formation and the role of silver nitrate was only to facilitate the formation of Au NPs/NWs. To further establish characteristic of Au NPs and NWs, the prepared gold nanoparticles were analyzed by X-Ray Diffraction (XRD) technique (see Fig. 3A). The X-ray diffractograms were similar for both Au NWs and NPs prepared at four different temperatures. The characteristic peaks at 38.269°, 44.600°, 64.678°, 77.549° are assigned to the (111), (200), (220), and (311) reflections of face centered cubic unit cell, which are typical for Au particles [67,68]. The difference in the peak intensity suggests highly crystalline nature of the Au NWs compared to the Au NPs, which could be due to the variation in shape at different temperatures.

Curcumin and CTAB capping with NPs/NWs were studied by FT-

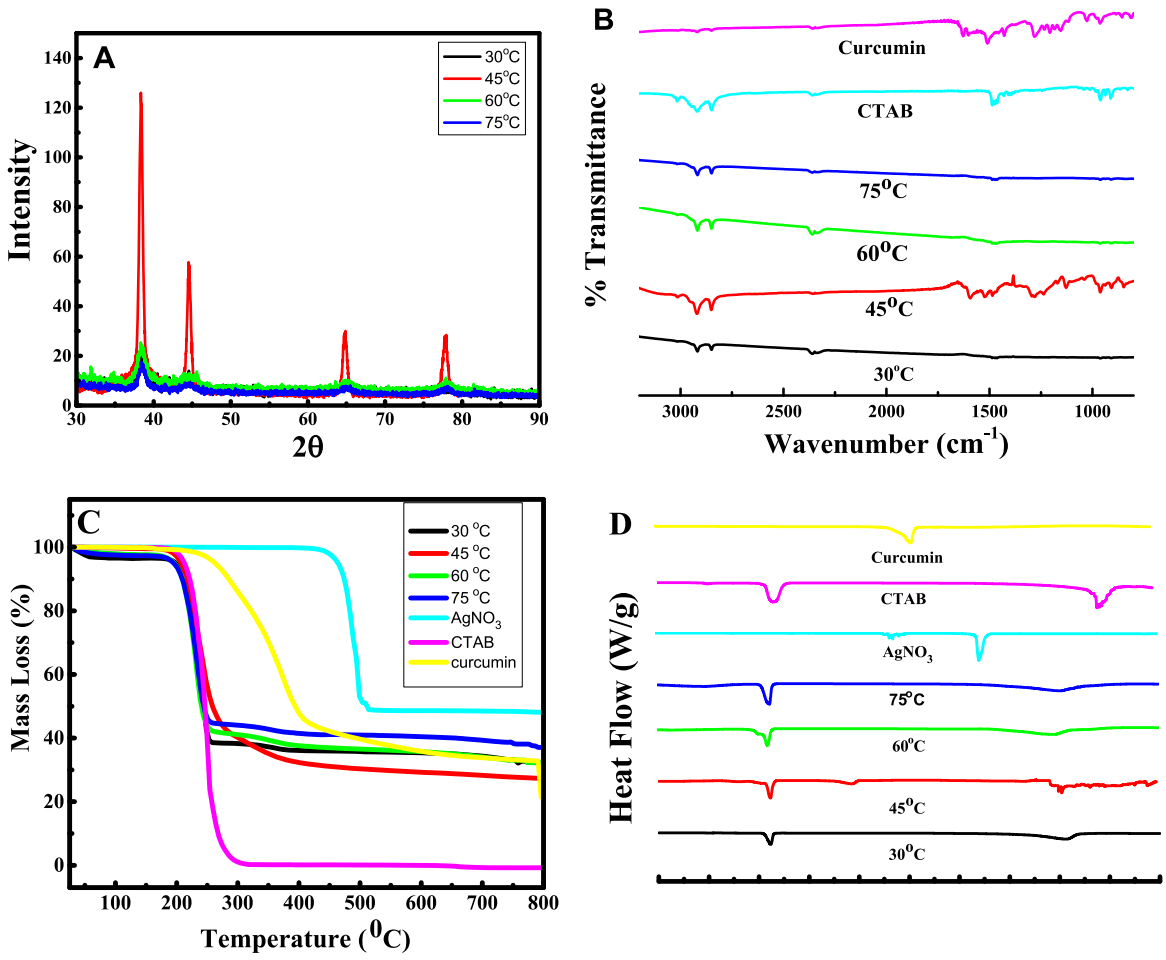

Fig. 3. (A) X-ray diffraction pattern of curcumin conjugated gold nanoparticles/nanowires prepared at 30, 45, 60 and 75 °C; (B) FT-IR spectra of CTAB, curcumin and curcumin conjugated gold nanoparticles (Au NPs) and nanowires (Au NWs) prepared at 30, 45, 60 and 75 °C; (C) TGA of CTAB, curcumin, silver nitrate and curcumin conjugated Au NPs and Au NWs prepared at 30, 45, 60 and 75 °C; (D) DSC curve of CTAB, curcumin, silver nitrate and curcumin conjugated Au NPs and Au NWs prepared at 30, 45, 60 and 75 °C.

IR. The FT-IR spectra for pure CTAB, Au NWs prepared at different temperature and pure curcumin are compared in Fig. 3B. In the spectral region 3200–2500 cm^{-1}, the C–H symmetric (stretching) and asymmetric (anti-stretching) vibration frequency modes at 2850 and 2919 cm^{-1} were seen for pure CTAB respectively meaning that it is a crystalline phase, which is distinguished from a micelle conformation. For pure CTAB, less intense peaks were observed at 3014, 1491 and 1453 cm^{-1} attributed to the asymmetric and symmetric C-H scissoring vibrations of CH_3-N^+ moieties and to the CH_2 scissoring mode. The region 1300–1680 cm^{-1} also signifies due to CH_2 scissoring mode of vibration. All these sharp peaks in pure CTAB were also present or slightly shifted but with low intensity in the case of the gold nanowires, which indicates an interaction of CTAB and the Au NWs surface. Concerning the FT-IR spectrum of curcumin, the strong peak at 1630 cm^{-1} has a predominantly mixed ν(C-C) and ν(C=O) character. Another strong band at 1601 cm^{-1} is attributed to the symmetric aromatic ring stretching vibrations ν(C C_{ring}). The 1519 cm^{-1} peak is assigned to the (C=O). Enol C-O peak was obtained at 1262 cm^{-1}, C-O-C peak at 1018 cm^{-1}, benzoate trans-CH vibration at 978 cm^{-1} and cis CH vibration of aromatic ring at 703 cm^{-1}. The bands at 1404 cm^{-1} represent the in-plane bending of the hydroxyl groups of the phenolic group. All the three bands (1404, 1262 and 978 cm^{-1}) were completely absent in the FT-IR spectrum of Au NWs, which suggests the interaction of $HAuCl_4$ at these sites. The bands at 774 cm^{-1} and 1424 cm^{-1} corresponding to the olefinic in-plane bending vibrations of the heptadiene chain of curcumin were observed in Au NWs demonstrating the presence of intact curcumin moiety in the Au NWs. Thus, it is obvious that in NWs prepared at 45 °C the Au NWs surface interact more than the gold nanoparticles formed at 30, 60 and 75 °C. The bands at 2926 cm^{-1}, 1471 cm^{-1}, 1045 cm^{-1} and 964 cm^{-1} that appeared in Au NWs are due to vibrations of aliphatic C–H stretches and mixed vibrations of CH_3, aromatic CCC and CCH of curcumin confirming the action of curcumin as a capping agent [49,69,70].

Thermogravimetric analysis given in Fig. 3C showed decomposition of CTAB, curcumin and $AgNO_3$ at ~279 °C [71], ~400 °C [72] and ~470 °C [73] respectively, which is consistent with other reported values. TGA data obtained for particles prepared in all the temperatures illustrated similar degradation pattern. However, for NWs prepared at 45 °C a significant weight loss of ~50% was found at ~300 °C, which is greater than the other temperatures (weight loss ~40%) indicating that the Au NWs are slightly richer in CTAB capping compared to NPs. Some of this weight loss could be due to the presence of curcumin too. Additionally, a ~10% weight loss for Au NPs/NWs between 300 °C and 400 °C is due to curcumin alone. Besides that, it is remarkable that no loss of water molecule around 100 °C for NPs/NWs prepared in 45, 60 and 75 °C which can be assumed that the samples are dehydrated in contrary to the nanoparticles formed at 30 °C where a loss of ~10% of water molecule is noticed. However, this also indicates that the NWs formed at 45 °C are more stable where the organic compounds are being more degraded and no loss in water is generated [49]. The DSC curves for the gold nanoparticles prepared at different temperatures, $AgNO_3$, CTAB and curcumin are shown in Fig. 3D. For NWs prepared at 45 °C, three endothermic peaks were

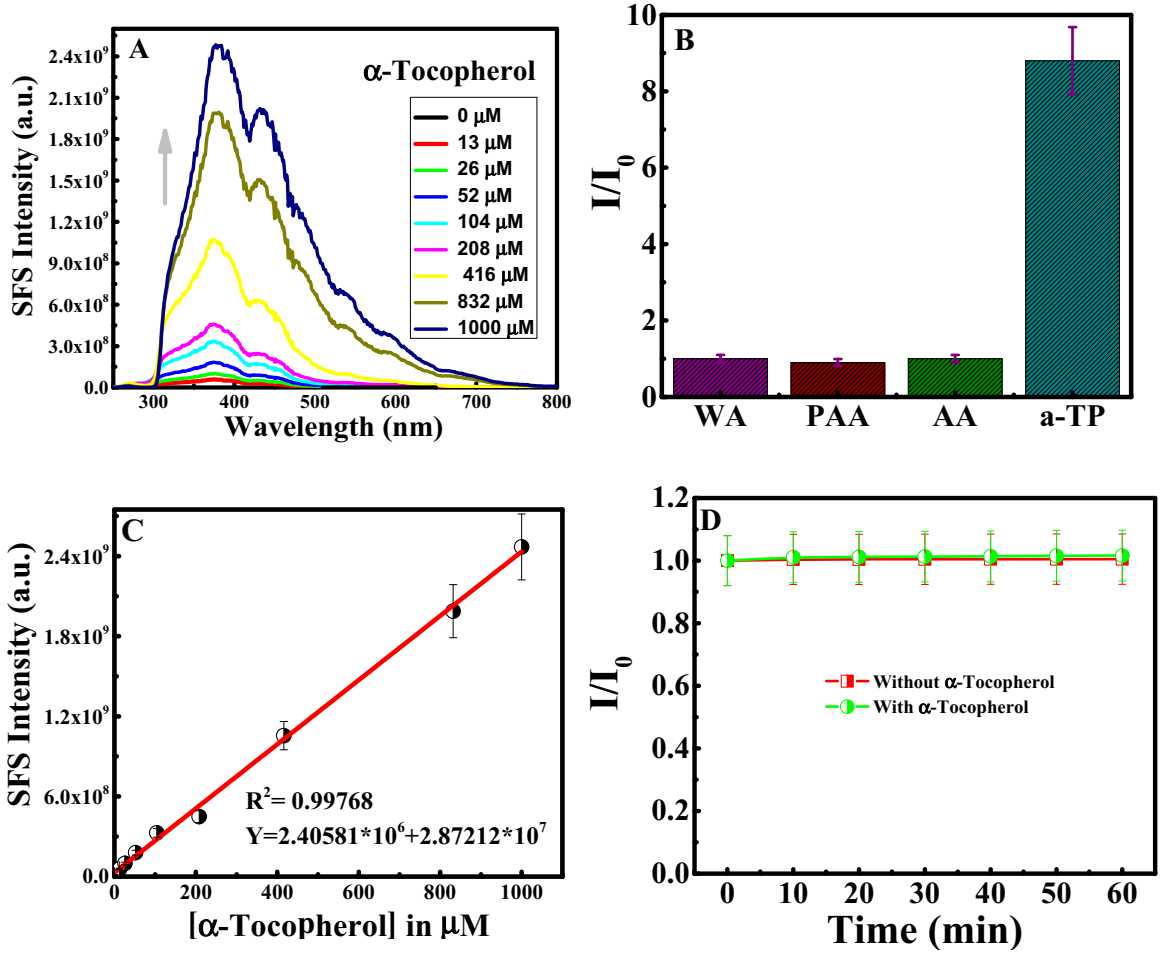

Fig. 4. (A) Synchronous fluorescence spectra (SFS) at Δλ=0 nm of curcumin conjugated Au NWs with different concentration of α-tocopherol; (B) Ratio of SFS intensity (I/I_0) of Au NWs for different species where WA (in absence of antioxidant), PAA: 6-O-Palmitoyl-L-ascorbic acid, AA: ascorbic acid, a-TP: α-tocopherol; (C) Linear correlation of SFS intensity of Au NWs vs. concentration of α-tocopherol; (D) Plot of I/I_0 of curcumin conjugated nanowires with time in the absence and presence of α-tocopherol.

obtained, ~106 °C and ~250 °C were similar to NPs obtained in other temperatures and an additional one at ~146 °C. These peaks were compared with that of CTAB and curcumin. DSC curve for CTAB showed a peak at ~106 °C similar with the peak obtained for the Au NWs indicating a solid-solid transition [71] and it's due to the melting temperature of CTAB tails in consequence of transition from order to disorder state [74]. The second peak at ~270 °C is attributed to decomposition of CTAB molecules, thus, the peaks at ~250 °C might be due to decomposition of CTAB molecules from the Au surfaces. Curcumin did not show any phase transition in this temperature range except an endothermic peak at 178 °C, which is as per reported literature [72]. The endothermic peak at ~146 °C for the procedure prepared at 45 °C can be due to desorption of free and uncomplexed CTAB/curcumin molecules. Finally, DSC curve for $AgNO_3$ gave an endothermic peak at ~210 °C which is unique for Ag and not found in the DSC curves relative to the AuNPs/AuNWs. This, further verified earlier EDX observation that role of $AgNO_3$ is only to facilitate formation of Au NWs/NPs.

At present, gold nanoparticles can be used as probes or biochemical sensors only if they are modified chemically with organic compounds [75]. In fact, as probes, gold nanoparticles should respond to the changes of their molecular environment, and as essential parts of the sensors, they should be coupled to recognition units and respond to target binding by the change of parameters of their resonance Rayleigh scattering. Ideally, this response should be independent of their concentration, and the valuable information should be derived from the concentration independent change of their RRS parameters [76]. In the field of nanoparticles research and analytical chemistry, RRS spectra are recently being utilized [66,77]. The principle behind these phenomena is elastic scattering. RRS is produced when the wavelength of Rayleigh scattering is located at or close to the molecular absorption band [77]. When the analyte interacts with the probe, the intensity of RRS is greatly increased. This is a simple technique and has been successfully used for nanoparticles earlier [62,66,78,79].

Since optimum enhancement of RRS signal is crucial for higher sensitivity during bio-sensing, Au nanowires prepared at 45 °C was chosen for sensing α-tocopherol, which is the predominant vitamin E form in tissues and is the least catabolized [80]. Excitingly, addition of α-tocopherol remarkably, about 10-fold, changed the RRS signal of Au NWs as shown in Fig. 4A. However, the spectral shape and RRS wavelength maximum remained constant. This appreciable change in RRS signal could be due to complexation of α-tocopherol with Au NWs through a non-covalent interaction. To test it further, other potential anti-oxidant interference from various substances was tested. Ascorbic acid and 6-O-palmitoyl-L-ascorbic acid could interfere during estimation of α-tocopherol. As confirmed from Fig. 4B, 30 μmol L^{-1} of ascorbic acid or 6-O-palmitoyl-L-ascorbic acid did not alter the RRS signal of Au NWs unlike ~9-fold increase observed for same concertation of α-tocopherol. The boost in RRS signal of Au NWs in the presence of α-tocopherol indicates larger complex formation by association of Au NWs with α-tocopherol, this could be similar to complexation of Au NPs with DNA in the presence of Al^{3+} [48], which

Table 1
Recovery results of the method.

	Theoretical Concentration (μmol L^{-1})	Experimental Concentration (μmol L^{-1})	Recovery (%)
Unknown 1	200	192.5 ± 1.8	96.3
Unknown 2	100	98.1 ± 2.2	98.1
Unknown 3	50	46 ± 1.6	92

is further facilitated by curcumin conjugation at the surface of Au NWs through hydrophobic interaction. However, presence of glutathione and cysteine in the samples may interfere due to formation of Au-S bond, nevertheless, these interfering chemicals are often not found along with α-tocopherol.

Comprehending the significance of Au NWs for selective sensing of α-tocopherol, the calibration curve was made by measuring RRS single of Au NWs in different concentration of α-tocopherol. The RRS spectra of Au NWs in the presence of different concentrations of α-tocopherol is shown in Fig. 4A, at very low concentration of 12.8 μmol L^{-1} to high concentration of 1.00 mmol L^{-1} there was no change in the shape of RRS spectra of Au NWs, however, the RRS signal continuously increased with the concentration of α-tocopherol. The RRS signal alteration of Au NWs with α-tocopherol concentration is plotted in Fig. 4C. As can be seen in the plot, in a wide range of concentration range, the curve showed linear change. This linear increase was very well fitted with a linear equation, $Y=2.41\times10^{6}+2.87\times10^{7}$ with $R^2=0.998$. Such a good correlation justifies the applicability of the present method for the determination of α-tocopherol in the given concentration range. The detection limit was estimated to be 50 nmol L^{-1}. Most of the available methods for α-tocopherol estimation work in lower concentration range. Brabcová et al. [81] and Korchazhkina et al. [82] have reported a linear dynamic range of 117–700 μmol L^{-1} and 16.7–65 μmol L^{-1}, giving a limit of detection equal to 1.35 and 1.51 μmol L^{-1} respectively using high performance liquid chromatography. Xinlei et al. [83] have reported a linear dynamic range of 117–583 μmol L^{-1}. Sadilek et al. [84] have found a linear dynamic range of 3–50 μmol L^{-1}. However, majority of the reported methods are based on separation technique like HPLC, electrophoresis or GC and the one without any separation method reported is using electrochemical method, which works in the range 0.5–90 μmol L^{-1} [55]. However, the present method showed a wider linear dynamic range between 12.8–1004 μmol L^{-1} with lowest limit of detection equal to 50 nmol L^{-1}. For testing applicability, synthetic samples of α-tocopherol were prepared and the concentrations were estimated using calibration curve obtained from this developed method. The obtained results in the form of percentage of recovery (% of recovery) are summarized in Table 1, which is quite acceptable. The stability of Au NWs is illustrated in Fig. 4D. When RRS signal of Au NWs was recorded in the absence and presence of α-tocopherol for one hour, the signal was found to be remarkably stable indicating the current sensor is quite stable during measurement time.

4. Conclusion

Curcumin capped gold nanowires was prepared using a green method where Au^{3+} ions were reduced to Au^{0} in presence of curcumin in CTAB micelle. The synthesis was carried out at different temperatures and temperature could able to manipulate size and shape of Au particles during green synthesis. Interestingly, thin and long NWs of ~20 nm to 25 nm diameter and >1 μm length could be prepared at 45 °C, however, decreasing synthesis temperature to 30 °C did not form any nanowires rather than smaller spherical nanoparticles. Increasing the synthesis temperature to 60 or 75 °C formed broken nanowires and spherical nanoparticles. Curcumin along with CTAB acted as capping and stabilizing agent for Au NWs/NPs. Resonance Rayleigh scattering signal could be amplified by forming into longer Au nanowires instead of spherical nanoparticles. Mixture of Au NWs and NPs or shorter NWs did not show any enhancement in the signal indicating formation of longer NWs is crucial for optimal enhancement of RRS signal. The amplified RRS signal of Au NWs could be successfully exploited to design an optical biosensor for α-tocopherol. Binding of α-tocopherol with Au NWs further boosted the RRS signal of Au NWs, this enhancement was ~10 fold through a non-covalent interaction that is encouraged by curcumin conjugation at the surface of Au NWs. There was no interference from other antioxidant substances like ascorbic acid and 6-O-Palmitoyl-L-ascorbic acid even at concentration of 30 μmol L^{-1}. The proposed sensing method offered remarkable linear dynamic ranges, 12.8–1004 μmol L^{-1}, which is larger than reported values. The detection limit for α-TOH estimation was 50 nmol L^{-1}. The proposed biosensor was stable both in the absence and presence of α-TOH and gave an excellent recovery for synthetic samples, thus, RRS signal can be tuned by controlling size and shape of the metallic nanoparticles to design novel bio-sensing techniques, which are simple, fast and sensitive.

Acknowledgment

Financial support provided by Lebanese National Council of Scientific Research (NCSR), Lebanon and American University of Beirut, Lebanon through URB as well as Kamal A. Shair Central Research Laboratory (KAS CRSL) facilities to carry out this work is greatly acknowledged.

References

[1] Y. Xia, N.J. Halas, Shape-controlled synthesis and surface plasmonic properties of metallic nanostructures, MRS Bull. 30 (2011) 338–348.
[2] D. Patra, R. Aridi, K. Bouhadir, Fluorometric sensing of DNA using curcumin encapsulated in nanoparticle-assembled microcapsules prepared from poly(diallylammonium chloride-co-sulfur dioxide), Microchim. Acta 180 (2013) 59–64.
[3] R.N. Moussawi, D. Patra, Modification of nanostructured ZnO surfaces with curcumin: fluorescence-based sensing for arsenic and improving arsenic removal by ZnO, RSC Adv. 6 (2016) 17256–17268.
[4] M. Mouslmani, K.H. Bouhadir, D. Patra, Poly (9-(2-diallylaminoethyl)adenine HCl-co-sulfur dioxide) deposited on silica nanoparticles constructs hierarchically ordered nanocapsules: curcumin conjugated nanocapsules as a novel strategy to amplify guanine selectivity among nucleobases, Biosens. Bioelectron. 68 (2015) 181–188.
[5] V.V. Mody, R. Siwale, A. Singh, H.R. Mody, Introduction to metallic nanoparticles, J. Pharm. Bioallied Sci. 2 (2010) 282–289.
[6] O. Masala, R. Seshadri, Synthesis routes for large volumes of nanoparticles, Annu. Rev. Mater. Res. 34 (2004) 41–81.
[7] M.C.M. Daniel, D. Astruc, Gold nanoparticles: assembly, supramolecular chemistry, quantum-size related properties and applications toward biology, catalysis and nanotechnology, Chem. Rev. 104 (2004) 293–346.
[8] S. Link, M.A. El-Sayed, Size and temperature dependence of the plasmon absorption of colloidal gold nanoparticles, J. Phys. Chem. B 103 (1999) 4212.
[9] T.K. Sau, C.J. Murphy, Room temperature, high-yield synthesis of multiple shapes of gold nanoparticles in aqueous solution, J. Am. Chem. Soc. 126 (2004) 8648–8649.
[10] Z.C. Xu, C.M. Shen, C.W. Xiao, T.-Z. Yang, H.-R. Zhang, J.-Q. Li, H.-L. Li, H.-J. Gao, Wet chemical synthesis of gold nanoparticles using silver seeds: a shape control from nanorods to hollow spherical nanoparticles, Nanotechnology 18 (2007) 115608.
[11] C.J. Murphy, T.K. Sau, A.M. Gole, C.J. Orendorff, J. Gao, L. Gou, S.E. Hunyadi, T. Li, Anisotropic metal nanoparticles: synthesis, assembly, and optical applications, J. Phys. Chem. B 109 (2005) 13857–13870.
[12] E. Boisselier, D. Astruc, Gold nanoparticles in nanomedicine: preparations, imaging, diagnostics, therapies and toxicity, Chem. Soc. Rev. 38 (2009) 1759–1782.
[13] D.A. Giljohann, D.S. Seferos, W.L. Daniel, M.D. Massich, P.C. Patel, C.A. Mirkin, Gold nanoparticles for biology and medicine, Angew. Chem. Int. Ed. 49 (2010) 3280–3294.
[14] P.K. Jain, K.S. Lee, I.H. El-Sayed, M.A. El-Sayed, Calculated absorption and scattering properties of gold nanoparticles of different size, shape, and composition: applications in biological imaging and biomedicine, J. Phys. Chem. B 110 (2006) 7238–7248.
[15] E.C. Dreaden, A.M. Alkilany, X. Huang, C.J. Murphy, M.A. El-Sayed, The golden age: gold nanoparticles for biomedicine, Chem. Soc. Rev. 41 (2012) 2740.
[16] X. Huang, P.K. Jain, I.H. El-sayed, M.A. El-Sayed, Gold nanoparticles: interesting

optical properties and recent applications in cancer diagnostics and therapy, Nanomedicine 2 (2007) 681–693.
[17] J. Yguerabide, E.E. Yguerabide, Light-scattering submicroscopic particles as highly fluorescent analogs and their use as tracer labels in clinical and biological applications, Anal. Biochem. 262 (1998) 157–176.
[18] C.J. Orendorff, S.C. Baxter, E.C. Goldsmith, C.J. Murphy, Light scattering from gold nanorods: tracking material deformation, Nanotechnology 16 (2005) 2601–2605.
[19] G. Raschke, S. Kowarik, T. Franzl, C. Sönnichsen, T.A. Klar, J. Feldmann, Biomolecular recognition based on single gold nanoparticle light scattering, Nano Lett. 3 (2003) 935–938.
[20] C.Z. Li, K.B. Male, S. Hrapovic, J.H.T. Luong, Fluorescence properties of gold nanorods and their application for DNA biosensing, Chem. Commun. 2005 (2005) 3924–3926.
[21] K. Imura, T. Nagahara, H. Okamoto, Plasmon mode imaging of single gold nanorods, J. Am. Chem. Soc. 126 (2004) 12730–12731.
[22] A. Mooradian, Photoluminescence of metals, Phys. Rev. Lett. 22 (1969) 185–187.
[23] I. Nabiev, I. Chourpa, M. Manfait, Applications of Raman and surface-enhanced Raman scattering spectroscopy in medicine, J. Raman Spectrosc. 25 (1994) 13–23.
[24] T.M. Cotton, J. Kim, Application of surface-enhanced Raman spectroscopy to biologica systems, J. Raman Spectrosc. 22 (1991) 729–742.
[25] G.C. Schatz, Theoretical studies of surface enhanced Raman scattering, Acc. Chem. Res. 17 (1984) 370–376.
[26] V.P. Zharov, E.N. Galitovskaya, C. Johnson, T. Kelly, Synergistic enhancement of selective nanophotothermolysis with gold nanoclusters: potential for cancer therapy, Lasers Surg. Med. 226 (2005) 219–226.
[27] C.M. Pitsillides, E.K. Joe, X. Wei, R.R. Anderson, C.P. Lin, Selective cell targeting with light-absorbing microparticles and nanoparticles, Biophys. J. 84 (2003) 4023–4032.
[28] X. Huang, P.K. Jain, I.H. El-sayed, M.A. El-Sayed, Determination of the minimum temperature required for selective photothermal destruction of cancer cells with the use of immunotargeted gold nanoparticles, Photochem. Photobiol. (2006) 412–417.
[29] M. Shah, V. Badwaik, Y. Kherde, H.K. Waghwani, T. Modi, Z.P. Aguilar, H. Rodgers, W. Hamilton, T. Marutharaj, C. Webb, M.B. Lawrenz, R. Dakshinamurthy, Gold nanoparticles: various methods of synthesis and antibacterial applications, Front. Biosci. 19 (2014) 1320–1344.
[30] K.B. Narayanan, N. Sakthivel, Phytosynthesis of gold nanoparticles using leaf extract of Coleus amboinicus Lour, Mater. Charact. 61 (2010) 1232–1238.
[31] V. Reddy, R.S. Torati, S. Oh, C. Kim, Biosynthesis of gold nanoparticles assisted by Sapindus mukorossi Gaertn. Fruit pericarp and their catalytic application for the reduction of p-nitroaniline, Ind. Eng. Chem. Res. 52 (2013) 556–564.
[32] J.Y. Song, H.K. Jang, B.S. Kim, Biological synthesis of gold nanoparticles using Magnolia kobus and Diopyros kaki leaf extracts, Process Biochem. 44 (2009) 1133–1138.
[33] L. Du, H. Jiang, X. Liu, E. Wang, Biosynthesis of gold nanoparticles assisted by Escherichia coli DH5α and its application on direct electrochemistry of hemoglobin, Electrochem. Commun. 9 (2007) 1165–1170.
[34] M. Agnihotri, S. Joshi, A.R. Kumar, S. Zinjarde, S. Kulkarni, Biosynthesis of gold nanoparticles by the tropical marine yeast Yarrowia lipolytica NCIM 3589, Mater. Lett. 63 (2009) 1231–1234.
[35] K. Bosecker, Bioleaching: metal solubilization by microorganisms, FEMS Microbiol. Rev. 20 (1997) 591–604.
[36] K.B. Narayanan, N. Sakthivel, Facile green synthesis of gold nanostructures by NADPH-dependent enzyme from the extract of Sclerotium rolfsii, Colloids Surf. A Physicochem. Eng. Asp. 380 (2011) 156–161.
[37] M.R. Johan, L.C. Chong, N.A. Hamizi, Preparation and stabilization of monodisperse colloidal gold by reduction with monosodium glutamate and poly (Methyl methacrylate), Int. J. Electrochem. Sci. 7 (2012) 4567–4573.
[38] N. Basu, R. Bhattacharya, P. Mukherjee, Protein-mediated autoreduction of gold salts to gold nanoparticles, Biomed. Mater. 3 (2008) 034105.
[39] R.C. Srimal, B.N. Dhawan, Pharmacology of diferuloyl methane (curcumin), a non-steroidal anti-inflammatory agent, J. Pharm. Pharmacol. 25 (1973) 447–452.
[40] A. Khafif, S.P. Schantz, T.C. Chou, D. Edelstein, P.G. Sacks, Quantitation of chemopreventive synergism between (-)-epigallocatechin-3-gallate and curcumin in normal, premalignant and malignant human oral epithelial cells, Carcinogenesis 19 (1998) 419–424.
[41] T. Ak, I. Gülçin, Antioxidant and radical scavenging properties of curcumin, Chem. Biol. Interact. 174 (2008) 27–37.
[42] R.A. Sharma, A.J. Gescher, W.P. Steward, Curcumin: the story so far, Eur. J. Cancer 41 (2005) 1955–1968.
[43] M. Chebl, M.G. Abiad, Z. Moussa, D. Patra, Two modes of associations of curcumin with pre- and nanoaggregated chitosan oligosaccharide lactate: ionic strength and hydrophobic bile salt modulate partition of drug and self-assembly process, J. Phys. Chem. C 120 (2016) 11210–11224.
[44] Z. Moussa, M. Hmadeh, M.G. Abiad, O.H. Dib, D. Patra, Encapsulation of curcumin in cyclodextrin-metal organic frameworks: dissociation of loaded CD-MOFs enhances stability of curcumin, Food Chem. 212 (2016) 485–494.
[45] M. Balasubramanyam, A.A. Koteswari, R.S. Kumar, S.F. Monickaraj, J.U. Maheswari, V. Mohan, Curcumin-induced inhibition of cellular reactive oxygen species generation: novel therapeutic implications, J. Biosci. 28 (2003) 715–721.
[46] H. Hatcher, R. Planalp, J. Cho, F.M. Torti, S.V. Torti, Curcumin: from ancient medicine to current clinical trials, Cell. Mol. Life Sci. 65 (2008) 1631–1652.
[47] R.N. Moussawi, D. Patra, Synthesis of Au nanorods through prereduction with curcumin: preferential enhancement of Au nanorod formation prepared from CTAB-capped over citrate-capped Au seeds, J. Phys. Chem. C 119 (2015) 19458–19468.
[48] D. Patra, R.N. Moussawi, Curcumin conjugated gold nanoparticles for nucleic acid sensing, in: Proceedings of the IEEE 15th International Conference on Nanotechnology, IEEE-NANO 2015, 2016, pp. 401–404.
[49] R. El Kurdi, D. Patra, Role of OH- in the formation of highly selective gold nanowires at extreme pH: multi-fold enhancement in rate of catalytic reduction reaction by gold nanowires, Phys. Chem. Chem. Phys. 19 (2017) 5077–5090. http://dx.doi.org/10.1039/c6cp08607a.
[50] K. Sindhu, A. Rajaram, K.J. Sreeram, R. Rajaram, Curcumin conjugated gold nanoparticle synthesis and its biocompatibility, RSC Adv. 4 (2014) 1–11.
[51] C.K. Sen, S. Khanna, C. Rink, S. Roy, Tocotrienols: the emerging face of natural vitamin E, Vitam. Horm. 76 (2007) 203–261.
[52] J.L. Buttriss, A.T. Diplock, High-performance liquid chromatography methods for vitamin E in tissues, Methods Enzymol. 105 (1984) 131–138.
[53] D.B. Parrish, Determination of vitamin E in foods–a review, Crit. Rev. Food Sci. Nutr. 13 (1980) 161–187.
[54] R.R. Eitenmiller, W.O. Landen, L. Ye, Vitamin Analysis for the Health and Food Sciences, Second ed., CRC Press, Boca Raton, FL, 2007, p. 664.
[55] J. Pokorny, N. Yanishlieva, M. Gordon, Antioxidants in Food Preservation: Practical Application, 1st ed., Woodhead Publishing, Boca Raton, FL, 2001.
[56] H. Filik, A.A. Avan, S. Aydar, Ş. Çakar, Determination of tocopherol using reduced graphene oxide-nafion hybrid-modified electrode in pharmaceutical capsules and vegetable oil samples, Food Anal. Methods 9 (2016) 1745–1753.
[57] F.J. Rupérez, D. Martín, E. Herrera, C. Barbas, Chromatographic analysis of α-tocopherol and related compounds in various matrices, J. Chromatogr. A 935 (2001) 45–69.
[58] T. Galeano-Díaz, M.I. Acedo-Valenzuela, A. Silva-Rodríguez, Determination of tocopherols in vegetable oil samples by non-aqueous capillary electrophoresis (NACE) with fluorimetric detection, J. Food Compos. Anal. 25 (2012) 24–30.
[59] L. Shang, H. Chen, L. Deng, S. Dong, Enhanced resonance light scattering based on biocatalytic growth of gold nanoparticles for biosensors design, Biosens. Bioelectron. 23 (2008) 1180–1184.
[60] X. Luo, A. Morrin, A.J. Killard, M.R. Smyth, Application of nanoparticles in electrochemical sensors and biosensors, Electroanalysis 18 (2006) 319–326.
[61] L. Vigderman, B.P. Khanal, E.R. Zubarev, Functional gold nanorods: synthesis, self-assembly, and sensing applications, Adv. Mater. 24 (2012) 4811–4841.
[62] J.-H. Lin, W.-L. Tseng, Ultrasensitive detection of target analyte-induced aggregation of gold nanoparticles using laser-induced nanoparticle Rayleigh scattering, Talanta 132 (2015) 44–51.
[63] K.I. Priyadarsini, The chemistry of curcumin: from extraction to therapeutic agent, Molecules 19 (2014) 20091–20112.
[64] X. Huang, M.A. El-Sayed, Gold nanoparticles: optical properties and implementations in cancer diagnosis and photothermal therapy, J. Adv. Res. 1 (2010) 13–28.
[65] C. Lertvachirapaiboon, A. Baba, S. Ekgasit, C. Thammacharoen, K. Shinbo, K. Kato, F. Kaneko, Gold nanoparticles synthesis used for sensor applications, Int. Symp. Electr. Insul. Mater. (2011) 395–397.
[66] E. El Khoury, M. Abiad, Z.G. Kassaify, D. Patra, Green synthesis of curcumin conjugated nanosilver for the applications in nucleic acid sensing and anti-bacterial activity, Colloids Surf. B Biointerfaces 127 (2015) 274–280.
[67] A.L. González-mendoza, L.I. Cabreralara, Reaction parameters for controlled sonosynthesis of gold nanoparticles, Chem. Soc. Rev. 59 (2015) 119–129.
[68] J. Li, H. Feng, Y. Feng, Y. Zhang, J. Jiang, D. Qian, Fabrication of gold nanoparticles-decorated reduced graphene oxide as a high performance electrochemical sensing platform for the detection of toxicant Sudan I, Electrochim. Acta 167 (2015) 226–236.
[69] S.R. Ede, U. Nithiyanantham, S. Kundu, Enhanced catalytic and SERS activities of CTAB stabilized interconnected osmium nanoclusters, Phys. Chem. Chem. Phys. 16 (2014) 22723–22734.
[70] R.B. Viana, A.B.F. Da Silva, A.S. Pimentel, Infrared spectroscopy of anionic, cationic, and zwitterionic surfactants, Adv. Phys. Chem. 2012 (2012) 903272.
[71] A. Swami, A. Kumar, M. Sastry, Formation of water-dispersible gold nanoparticles using a technique based on surface-bound interdigitated bilayers, Langmuir 19 (2003) 1168–1172.
[72] V.A. Marcolino, G.M. Zanin, L.R. Durrant, M.D.T. Benassi, G. Matioli, Interaction of curcumin and bixin with β-cyclodextrin: complexation methods, stability, and applications in food, J. Agric. Food Chem. 59 (2011) 3348–3357.
[73] J. Liu, J. Liu, W. Song, F. Wang, Y. Song, The role of electronic interaction in the use of Ag and Mn_3O_4 hybrid nanocrystals covalently coupled with carbon as advanced oxygen reduction electrocatalysts, J. Mater. Chem. A 2 (2014) 17477–17488.
[74] T. Zhang, G. Xu, J. Puckette, F.D. Blum, Effect of silica on the structure of cetyltrimethylammonium bromide, J. Phys. Chem. C 116 (2012) 11626–11634.
[75] S. Liu, Z. Yang, Z. Liu, L. Kong, Resonance Rayleigh-scattering method for the determination of proteins with gold nanoparticle probe, Anal. Biochem. 353 (2006) 108–116.
[76] H. Yao, Prospects for organic dye nanoparticles, in: A.P. Demchenko (Ed.), Advanced Fluorescence Reporters in Chemistry and Biology II: Molecular Constructions, Polymers and Nanoparticles 9 (2010), 2010, pp. 285–304.
[77] X. Long, H. Zhang, S. Bi, Frequency doubling scattering and second-order scattering spectra of phosphato-molybdate heteroply acid–protein system and their analytical application, Spectrochim. Acta Part A Mol. Biomol. Spectrosc. 60 (2004) 1631–1636.
[78] S.P. Liu, Z. Yang, Z.F. Liu, J.T. Liu, Y. Shi, Resonance Rayleigh scattering study on the interaction of gold nanoparticles with berberine hydrochloride and its analytical application, Anal. Chim. Acta 572 (2006) 283–289.
[79] C.C. Wang, M.O. Luconi, A.N. Masi, L.P. Fernández, Derivatized silver nanoparticles as sensor for ultra-trace nitrate determination based on light scattering

phenomenon, Talanta 77 (2009) 1238–1243.
[80] Q. Jiang, H. Freiser, K.V. Wood, X. Yin, Identification and quantitation of novel vitamin E metabolites, sulfated long-chain carboxychromanols, in human A549 cells and in rats, J. Lipid Res. 48 (2007) 1221–1230.
[81] I. Brabcová, L. Kovářová, D. Šatínský, L. Havlíková, P.A. Solich, Fast HPLC method for determination of vitamin E acetate in dietary supplements using monolithic column, Food Anal. Methods 6 (2013) 380–385.
[82] O. Korchazhkina, E. Jones, M. Czauderna, S.A. Spencer, J. Kowalczyk, HPLC with UV detection for measurement of vitamin E in human milk, Acta Chromatogr. 16 (2006) 48–57.
[83] Y. Xinlei, Y. Yanhai, L. Lang, X. Yao, Fast analysis of fat-soluble vitamins in infant milk powder by heart cutting 2D-LC, Food Test Agric. (2015) 1–6.
[84] P. Sadilek, D. Satinsky, M. Ot'apka, R. Sladkovsky, P. Solich, Rapid and simple determination of vitamin A and vitamin E in human plasma by column-switching high-performance liquid chromatography, Curr. Anal. Chem. 5 (2009) 311–315.